Proton and Electron Pathways in the Bacterial Nitric Oxide Reductase[†,⊥]

Janneke H. M. Hendriks,[‡,§] Audrius Jasaitis,[||] Matti Saraste,[‡] and Michael I. Verkhovsky*[,||]

European Molecular Biology Laboratory, Meyerhofstrasse 1, Postfach 102209, D-69012 Heidelberg, Germany, and Helsinki Bioenergetics Group, Institute of Biotechnology, P.O. Box 56 (Viikinkaari 5), University of Helsinki, 00014 Helsinki, Finland

Received November 29, 2001

ABSTRACT: Electron- and proton-transfer reactions in bacterial nitric oxide reductase (NOR) have been investigated by optical spectroscopy and electrometry. In liposomes, NOR does not show any generation of an electric potential during steady-state turnover. This electroneutrality implies that protons are taken up from the same side of the membrane as electrons during catalysis. Intramolecular electron redistribution after photolysis of the partially reduced CO-bound enzyme shows that the electron transfer in NOR has the same pathway as in the heme−copper oxidases. The electron is transferred from the acceptor site, heme *c*, via a low-spin heme *b* to the binuclear active site (heme b_3/Fe_B). The electron-transfer rate between hemes *c* and *b* is $(3 \pm 2) \times 10^4$ s^{-1}. The rate of electron transfer between hemes *b* and b_3 is too fast to be resolved ($>10^6$ s^{-1}). Only electron transfer between heme *c* and heme *b* is coupled to the generation of an electric potential. This implies that the topology of redox centers in NOR is comparable to that in the heme−copper cytochrome oxidases. The optical and electrometric measurements allow identification of the intermediate states formed during turnover of the fully reduced enzyme, as well as the associated proton and electron movement linked to the NO reduction. The first phase ($k = 5 \times 10^5$ s^{-1}) is electrically silent, and characterized by the disappearance of absorbance at 433 nm and the appearance of a broad peak at 410 nm. We assign this phase to the formation of a ferrous NO adduct of heme b_3. NO binding is followed by a charge separation phase ($k = 2.2 \times 10^5$ s^{-1}). We suggest that the formation of this intermediate that is not linked to significant optical changes involves movement of charged side chains near the active site. The next step creates a negative potential with a rate constant of $\sim 3 \times 10^4$ s^{-1} and a weak optical signature. This is followed by an electrically silent phase with a rate constant of 5×10^3 s^{-1} leading to the last intermediate of the first turnover (a rate constant of $\sim 10^3$ s^{-1}). The fully reduced enzyme has four electrons, enough for two complete catalytic cycles. However, the protons for the second turnover must be taken from the bulk, resulting in the generation of a positive potential in two steps. The optical measurements also verify two phases in the oxidation of low-spin hemes. Based on these results, we present mechanistic models of NO reduction by NOR. The results can be explained with a trans mechanism rather than a cis model involving Fe_B. Additionally, the data open up the possibility that NOR employs a P450-type mechanism in which only heme b_3 functions as the NO binding site during turnover.

The bacterial nitric oxide reductase (NOR)[1] is a membrane protein complex that catalyzes the reduction of nitric oxide to nitrous oxide according to the equation:

$$2NO + 2H^+ + 2e^- \rightarrow N_2O + H_2O$$

This reaction is part of the denitrification process that is used by bacteria as an alternative to oxygen-based respiration. Sequence analyses have indicated that NOR is a member of the superfamily of heme/copper cytochrome oxidases (*1*, *2*). Although the *nor* operon consists of four genes which might represent structural components (*3*), the active enzyme is purified as a two-subunit complex (NorBC) (*4*). The NorC subunit is a membrane-anchored cytochrome *c*. NorB is homologous to subunit I of the heme−copper oxidases. It contains one low-spin heme *b* and the binuclear active site (*5*, *6*). A high-spin B-type heme (heme b_3) and a non-heme iron called Fe_B form this binuclear site. Fe_B replaces Cu_B present in the active site of cytochrome oxidases (*7*).

Recently another type of NOR has been identified in *Ra. eutropha*. This enzyme consists of a single subunit and does not contain any cytochrome *c*. The electron donor for this enzyme is probably a membrane-soluble quinol (*8*, *9*). Genes

[†] This work was supported by grants from The Academy of Finland, The Sigrid Jusèlius Foundation, The University of Helsinki, and Biocentrum Helsinki.

* To whom correspondence should be addressed (Tel: +358919158005, Fax: +358919158001, E-mail: michael.verkhovsky@helsinki.fi).

[⊥] This paper is dedicated to the memory of Matti Saraste.

[‡] European Molecular Biology Laboratory.

[§] Present address: Max Planck Institute of Molecular Plant Physiology, Am Mühlenberg 1, D-14476 Golm, Germany.

[||] University of Helsinki.

[1] Abbreviations: CCO, cytochrome *c* oxidase; COMV, CO-bound mixed-valence state of the enzyme; COFR, CO-bound fully reduced state of the enzyme; NOR, nitric oxide reductase; OG, octyl-D-glucoside; RCR, respiratory control ratio; K^+-HEPES, *N*-(2-hydroxyethyl)piperazine-*N*′-2-ethanesulfonic acid; b_3, high-spin *b* heme; *b*, low-spin *b* heme; Fe_B, non-heme iron.

10.1021/bi0121050 CCC: $22.00
Published on Web 01/22/2002

with a high similarity to the latter enzyme have been identified in a number of bacterial genomes. Sequence analysis has indicated that both types of NOR arose as distinct subfamilies very early in evolution (*10*).

NOR is a very efficient scavenger of NO. The apparent K_m for NO is below 1 μM (*11*). During denitrification, such a high affinity allows the bacteria to keep the steady-state concentration of NO below the toxic level, typically <100 nM (*12*). At higher concentrations, the enzyme does not show normal Michaelis−Menten behavior. This has been attributed to substrate inhibition on the oxidized enzyme (*5*, *13*).

The mechanism by which NOR reduces NO is not known at present. All substrates of the reaction, NO, electrons, and protons, have to reach the active site of the enzyme. This site is probably buried inside the membrane, as in the case of heme−copper oxidases. For the single turnover of the enzyme, two NO molecules are required. EPR spectra of the enzyme during turnover have indicated that both iron atoms of the binuclear site in its reduced state can bind NO (*7*, *14*).

Equilibrium titrations of the redox centers have indicated that the midpoint potential of heme b_3 is only +60 mV, whereas the other redox centers have midpoint potentials between +250 and +350 mV (*15*). Until now, no results have been reported concerning the electron pathway and transfer rates inside the enzyme. The data on the proton consumption during catalysis suggest that the protons are taken up from the periplasm, that is, from the same side as the electrons [see (*16*)]. The details of the catalytic cycle have not been elucidated until now.

We have investigated the proton and electron pathways in NOR, using purified enzyme and enzyme reconstituted into liposomes. The electron-transfer reactions have been studied by electron redistribution after photolysis of CO from the partially reduced enzyme in the absence of NO. In addition, we have used the electrometric and spectrophotometric methods to study the catalytic intermediates and generation of $\Delta\Psi$ by NOR in the reaction of the reduced enzyme with NO after flash-induced release of CO from the inhibited enzyme.

MATERIALS AND METHODS

Protein Purification. NOR was purified from membranes of anaerobically grown *Paracoccus denitrificans* (*7*). The two-subunit aa_3-type cytochrome oxidase was purified from membranes of aerobically grown *Pa. denitrificans* MR-3 as described (*17*). Purified protein was frozen in liquid nitrogen and stored at −80 °C.

Preparation of NO Stock Solutions. NO stock solutions were prepared as described before (*7*). For optical and electrometric experiments, NO-saturated buffer was prepared on a vacuum/gas line from redistilled NO gas. For activity measurements, the purge method was used with commercial NO gas.

Preparation of CO-Mixed-Valence Enzyme. Samples were placed in rectangular cuvettes (5 optical windows) with internal dimensions of 4 × 10 mm, equipped with joints for attachment to the vacuum line. To prepare the CO-mixed-valence form of the enzyme, it is necessary to remove oxygen from the solution. This was done by repeatedly replacing the atmosphere in the cuvette with oxygen-free argon using a vacuum/gas line, followed by gentle rocking of the sample to equilibrate with the new atmosphere. Carbon monoxide (100%) was then introduced into the sample in a similar way to form the CO-mixed-valence form of the enzyme. Formation of the mixed-valence enzyme was monitored optically on a Unisoku single-beam spectrophotometer. The electrons needed for the partial reduction are generated by oxidation of CO ($CO + H_2O \rightarrow CO_2 + 2H^+ + 2e^-$). Prior to the beginning of the experiments, the atmosphere was exchanged with an argon gas mixture containing 1% or 10% CO, to slow further reduction as well as CO recombination, which is extremely fast in NOR [$k = 1.7 \times 10^8$ M^{-1} s^{-1}, (*18*)].

Transient Absorbance Measurements. Flash-induced transient absorption spectra were collected using a diode array spectrophotometer (Unisoku Instruments) equipped with a flash apparatus. This instrument can record spectra as rapidly as one per millisecond. The data form a surface containing the absorbance at 512 wavelengths at 512 time points. This surface was deconvoluted with SPLMOD, a global exponential fitting program, to obtain the initial difference spectrum and its relaxation rate. For a description of the basics of this software program, see (*19*).

Flash-induced rapid spectrophotometric measurements were carried out at a single wavelength at a time as described previously (*20*). For rapid optical measurements involving NO, the CO-bound protein sample was mixed with a saturated NO stock solution in a 1:1 ratio 100 ms prior to starting the reaction by a laser flash. Two-channel (sample/reference) data digitization involved a CompuScope 512 12-bit PC card (Gage Applied Sciences, Montreal, Canada), running data acquisition software written by Nikolai Belevich. The data were analyzed using SPLMOD after generating a surface of all traces at individual wavelengths.

Reconstitution. Reconstitution was accomplished using SM-2 Bio-Beads (BioRad) and preformed liposomes [after (*21*)] made from synthetic C-18 lipids (Avanti Polar Lipids, Alabaster, AL). The liposomes consisted of 56.5% phosphatidylglycerol, 34% phosphatidylcholine, 6% phosphatidylethanolamine, and 3.5% cardiolipin [mimicking the phospholipid composition in the native *Pa. denitrificans* membrane, (*22*)]. The mixture of phospholipids was dispersed in 100 mM K^+-HEPES, pH 7.4, and sized by repeated extrusion through a filter with 0.2 mm pores. The liposomes (approximately 5 mg of lipid/mL) were destabilized by incubation with 25 mM octyl-D-glucoside (OG) for 30 min. Purified protein was added to a total concentration of 0.5 μM from 100 μM solutions, and incubated for 1 more h. Removal of the detergent was achieved by three additions of Bio-Beads (30 mg/mL), with 2 h intervals. Each addition contained half the amount of Bio-Beads needed for total detergent removal that was estimated from the absorbance capacity of 117 mg of OG/g of Bio-Beads (*23*). All incubations were performed under nitrogen at room temperature. Proteoliposomes were used immediately for respiratory control tests or stored overnight on ice under argon for electrometric experiments.

Respiratory Control Ratio. The instrument described in (*7*) was used for measurements of oxygen concentrations. The NO reduction rate was measured using an ISO-NO electrode (World Precision Instruments, Berlin) in a 3.5 mL anaerobic chamber at 30 °C. The buffer contained 50 mM KCl, 50 mM K^+-HEPES, pH 7.4, 10 mM ascorbate, and

18.3−19.7 μM horse heart cytochrome *c*. The water-soluble nature of the reductant results only in the reduction of the enzyme population that has its electron acceptor side on the outside of the proteoliposomes. Consequently, only this population of enzyme can participate in turnover. In the oxidase assays, valinomycin and *p*-trifluoromethoxycarbonyl cyanide phenylhydrazone were used at 1 and 10 μM, respectively. In the NO reduction assay, the ionophore:lipid ratios were 1.3 times higher (actual concentration 3 times lower). Increasing the ionophore concentrations by a factor of 2.5 did not change their effects on NO reduction. The activities in the presence of the ionophores were approximately 430 e^-/s and 80 e^-/s for the oxygen and NO reduction, respectively.

Time-Resolved Electrometric Measurements of Membrane Potential Generation. The measurements are based on the method developed by Drachev and co-workers (*24*, *25*). In the present system, Ag/AgCl electrodes record the voltage between the two compartments of a cell that are separated by a membrane consisting of a lipid-impregnated Teflon mesh. Proteoliposomes containing NOR were associated with this membrane by a 2 h incubation in the presence of 20 mM calcium in 100 mM Bis-Tris propane, pH 7, after which calcium and unattached proteoliposomes were washed away, and the buffer was changed to 100 mM K^+-HEPES, pH 8. The voltage across the membrane is proportional to the membrane potential across the vesicle membranes, allowing the kinetics of charge translocation to be recorded. The method and the data collection setup are described in more detail in (*26*) and (*27*). Data were analyzed with MATLAB (Mathworks, South Natick, MA) using a sequential reaction model, as described in detail in (*27*).

Electrometric Measurements Involving NO. Generation of a membrane potential during steady-state turnover by NOR was tested by injection of low concentrations of NO (10−15 μM final concentration) into the stirred electrometric sample chamber, containing 100 mM K^+-HEPES, pH 8, 10 μM horse heart cytochrome *c*, and 5 mM ascorbate. The chamber had been made anaerobic by the presence of 50 mM glucose, 50 μg/mL catalase, and 130 μg/mL glucose oxidase in the medium under an atmosphere of argon.

"Flow−flash" type measurements require that NO is introduced into the sample shortly before the photolysis flash. In the electrometric apparatus, this was delivered through a long narrow needle positioned so that the jet from the needle was directed to the measuring membrane (a 4 mm circle), thus producing a high local concentration of NO during the initial time of the reaction. A computer-driven syringe pump (SP200i, World Precision Instruments) with a 2.5 mL gastight syringe was used; 100 μL portions of NO-saturated buffer were injected (5 mL/min) via a 450 mm 22S gauge RN needle (Hamilton, Reno, NV). The reaction was initiated by a flash from a frequency-doubled YAG laser (Quantel Brilliant; pulse energy 40 mJ). The diameter of the laser beam was 3.5 mm, so that over 75% of the membrane will be photolyzed.

The rate of CO dissociation from heme b_3 in NOR is unknown. Delivery of the entire 100 μL of NO-saturated buffer takes 1.2 s. The laser was fired before the nitric oxide injection had ended, typically 450 ms after the start of the injection, to prevent that the majority of the enzyme molecules will start to react with NO before the flash.

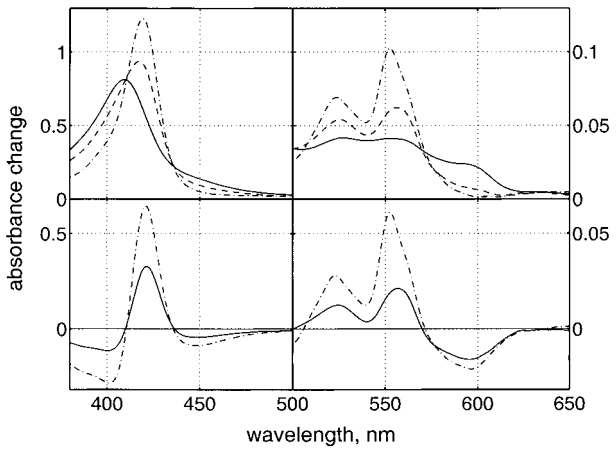

FIGURE 1: Optical spectra of NOR in 50 mM Tricine, pH 8, and 0.02% (w/v) DM in the oxidized state (—), mixed-valence state (COMV, − −), and fully reduced state with CO (COFR, − · −) (upper panels). The enzyme concentration was about 3 μM. The latter two samples contained 1 mM CO. The lower panels show the corresponding difference spectra: COMV minus oxidized (—) and COFR minus oxidized (− · −).

RESULTS

Internal Electron-Transfer Pathway and Transfer Rates

To understand the enzymatic mechanism of NO reduction, it is important to define and understand the electron pathway in the enzyme. This pathway can be investigated via the electron redistribution among the redox centers of partially reduced CO-bound enzyme after CO photolysis (this is so-called electron backflow). Such a reaction has been intensively studied with heme/copper oxidases (*28*−*30*). CO has much better binding to high-spin ferrous than ferric hemes. CO binding thus stabilizes the reduced state and thereby raises the heme's midpoint potential. This property of the hemes enables the formation of a CO-mixed-valence state in cytochrome oxidases, in which the active site is reduced, whereas the other metal centers are oxidized. Upon photolysis of the CO, the potential of the high-spin heme drops back to its basal value, causing redistribution of electrons between the heme and the other redox centers (*31*). Over time, the original mixed-valence state will re-form, due to the trapping of the electron on the high-spin heme by CO binding. From such transient electron redistribution, the internal electron pathway and rate constants of electron-transfer reaction can be determined.

Figure 1 shows the spectra of oxidized NOR, as well as partially and fully reduced NOR in the presence of 1 mM CO. The spectrum of oxidized NOR (solid line, Figure 1, upper panels) contains a very conspicuous band at 595 nm that has been ascribed as a charge-transfer band of the oxidized active site (*15*). Anaerobic incubation of this sample under CO results in the loss of this 595 nm band, indicating reduction of the active site. In the fully reduced sample, the reduction of the low-spin hemes *c* and *b* gives rise to the absorbance peak at 552 nm with a shoulder at 563 nm (Figure 1, lower panels). The absence of these features in the partially reduced enzyme shows that this sample is in the CO-mixed-valence state. Thus, NOR can spontaneously form this state in the presence of 1 mM CO.

Optical Backflow Measurements. Recombination of CO after photolysis of mixed-valence enzyme will include not

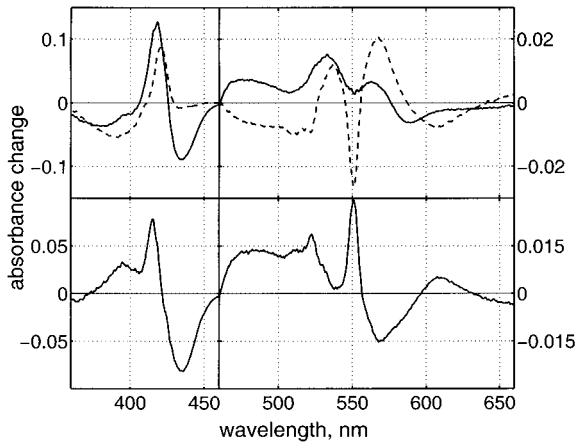

FIGURE 2: Spectral changes induced by flash photolysis on the NOR−CO complex. The sample contained 2.8 or 11.3 μM NOR (for the Soret and alpha band region experiments, respectively) in 50 mM Tricine buffer, pH 8.0, 0.02% (w/v) DM, and 10 μM CO. The upper panel shows the scaled difference spectrum obtained from a COMV sample of NOR (− −) and from the same sample after full reduction of NOR by addition of 100 μM dithionite (—). The lower panel shows the difference between these two spectra that represents the spectral changes that are caused solely by the electron transfer that occurs in COMV NOR after flash photolysis.

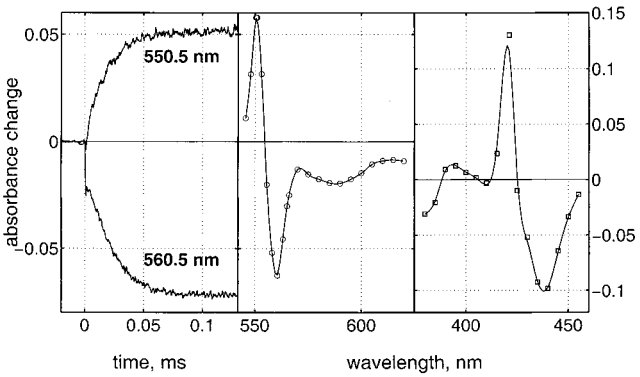

FIGURE 3: Kinetics of backflow in NOR. The left panel shows the initial time-resolved absorbance changes at 550.5 and 560.5 nm induced by a laser flash at $t = 0$ on a mixed-valence sample of NOR [29.3 μM NOR in 50 mM Tricine buffer, pH 8.0, 0.1% (w/v) DM, and 100 μM CO]. The traces represent the average of 50 measurements. The kinetic spectrum of the slower process seen is shown in the central panel. It was reconstructed by analyzing the amplitudes of this phase in traces recorded at various wavelengths. The right panel shows the kinetic spectrum reconstructed in a similar way in the Soret region using a mixed-valence sample containing 2.8 μM NOR under 10 μM CO. The rate constants of the kinetic spectra reconstructed were 4.8×10^4 and 2×10^4 s^{-1} in the visible and Soret region, respectively.

only CO rebinding but also the return of redistributed electrons to the high-spin heme b_3. Therefore, the spectrum of the CO-rebinding phase of the CO-mixed-valence enzyme contains the spectral changes induced by the binding of CO to the high-spin heme (i.e., the CO-binding spectrum) as well as the changes caused by the subsequent electron redistribution. The CO-binding spectrum can be determined by recording the spectral changes induced by photolysis of the fully reduced, CO-bound enzyme, in which no electron redistribution can occur after photolysis. The electron-transfer spectrum is obtained by subtracting the CO-binding spectrum from the mixed-valence data.

In the upper panel of Figure 2, the spectra obtained by photolysis on mixed-valence NOR (dashed line) and fully reduced NOR (solid line) are shown. The relaxation spectrum obtained with the mixed-valence sample was amplified by a factor 3.7, since the mixed-valence enzyme was found to contain only 27% of NOR in the CO-mixed-valence state.[2] The incomplete mixed-valence formation is partially due to the low concentration of CO in the sample (10 μM). The low midpoint potential of unliganded heme b_3 (*15*) causes the midpoint potential of the heme b_3−CO complex to be close to the midpoint potentials of the low-spin hemes. Due to this, the electrons reside on the low-spin hemes in the presence of low concentrations of CO in a fraction of the enzyme (not shown). We chose to work with low concentrations of CO in order to slow the CO recombination, which is extremely fast in NOR [$k_{on} = 1.7 \times 10^8$ M^{-1} s^{-1}, (*18*)].

[2] This percentage has been determined based on the amplitudes of the immediate change in absorbance induced by laser photolysis observed in rapid kinetic measurements (see Figure 7) that represents the CO-photolysis effect. The ratio of its amplitude in a mixed-valence sample to the amplitude obtained after complete reduction of the sample represents the CO-bound enzyme fraction. This fraction is enzyme in the CO-mixed-valence state, since CO only binds to the reduced heme, and the sample did not contain any fully reduced enzyme: the amplitude of the electron-transfer process still increased in parallel with the CO-photolysis amplitude over time.

The rate constants for the relaxation of the samples to the pre-photolysis state were 24 and 320 s^{-1} in the mixed-valence and fully reduced sample, respectively. A slower relaxation in the mixed-valence sample was expected, since CO can only recombine with a reduced heme b_3. The recombination is slowed in the mixed-valence enzyme due to the transient oxidation of heme b_3 by the electron backflow.

The difference between the kinetic spectra of the mixed-valence and fully reduced NOR is plotted in Figure 2, lower panel. This spectrum contains only the changes due to the electron transfer that occurs after photolysis in the CO-mixed-valence form of the enzyme. The troughs at 435 nm and around 570 nm and the positive peak at 608 nm show that the high-spin heme b_3 has been oxidized by the backflow. The absorbance at 608 nm is attributed to a charge-transfer band from the oxidized heme b_3 in the presence of reduced Fe_B (*15*). The sharp absorbance peaks at 420 and 551 nm are characteristic for reduction of *c*-type hemes.

Thus, backflow involves electron transfer between hemes b_3 and *c*. Based on the similarity to the cytochrome oxidases, the electron translocation between heme b_3 and heme *c* is expected to occur via heme *b*. In this case, the backflow would include two electron equilibration steps (heme b_3/heme *b* and heme *b*/heme *c*). The exact electron pathway and the rate constants of electron transfer can be determined by investigation of the kinetics of the backflow process.

Optical Backflow Kinetics. The left panel of Figure 3 shows the time-resolved absorbance changes at 550.5 and 560.5 nm, induced by flash photolysis on a mixed-valence sample of NOR. The data at 560.5 nm are clearly biphasic: an immediate response, caused by the instant disruption of the heme b_3−CO bond by the laser flash, is followed by a second phase of electron transfer with a time constant of ca. 20 μs ($k = 4.8 \times 10^4$ s^{-1}). To identify the nature of this electron equilibration process, its spectrum was reconstructed via analysis of its amplitude at various wavelengths between 545 and 620 nm (Figure 3, middle panel). The sharp peak

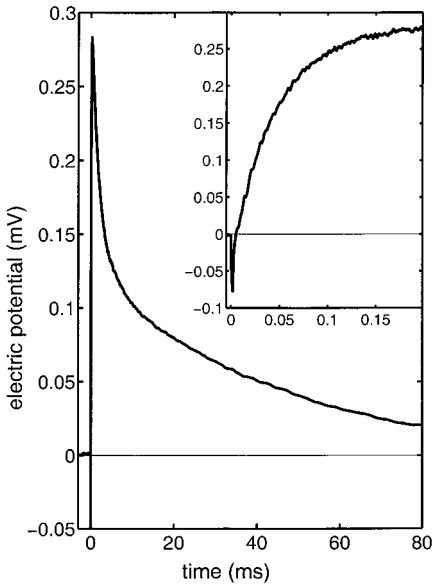

FIGURE 4: Electrogenic electron backflow of the COMV NOR. The main panel shows a typical recording, and the inset represents the first 200 μs of this process. The sample contained NOR-proteoliposomes in 100 mM Hepes−KOH, pH 8, 50 mM glucose, 50 μg/mL catalase, 130 μg/mL glucose oxidase, and 10 μM CO.

around 550 nm reveals reduction of heme *c*. The sharp trough at 560 nm indicates that the electron donor in this process is the low-spin heme *b*. The 20 μs phase thus represents electron equilibration between heme *b* and heme *c*. The interpretation is consistent with the data obtained in the Soret region (Figure 3, right panel).

In the CO-mixed-valence sample used in these experiments, only the active site of NOR appeared reduced, whereas the low-spin heme *b* seemed to be mainly oxidized. Thus, prior to the oxidation observed in the backflow, an electron coming from heme b_3 must have reduced heme *b*. This confirms that the electron-transfer pathway between heme *c* and heme b_3 is via heme *b*. The electron equilibration between heme b_3 and heme *b* was not detected, suggesting that it is too fast to be resolved in this experiment and, therefore, should have a time constant below 1 μs.

Our data show that the electron pathway in NOR is similar to that in the heme−copper cytochrome oxidases. The electrons are transferred from the acceptor site (heme *c*/Cu_A) via the low-spin heme in the catalytic subunit to the active site. We have investigated the backflow reaction by electrometry to test whether the topology of the redox centers is similar in NOR and cytochrome oxidases. Electrometry is a technique that gives a better time resolution and signal-to-noise ratio than the optical methods, and allows the detection of very fast and small charge movements across the membrane dielectric [see (*26*)].

Electrometric Backflow Measurements. Figure 4 shows the electrogenic backflow response induced by a laser flash on partially reduced, reconstituted NOR in the presence of 10 μM CO. After the laser flash at $t = 0$, some small negative potentials are transiently formed, followed by the generation of a positive potential with a rate constant of 1.9×10^4 s^{-1}. The potential relaxes in two phases with rate constants of 480 and 22 s^{-1}, respectively.

The rate constant of the major electrogenic phase identifies this phase as electron transfer between heme *b* and heme *c*. Since only the movement of electrons perpendicular to the membrane induces a potential, the large amplitude of this phase corroborates the idea that heme *b* resides well inside the membrane dielectric, and that heme *c* is located outside the membrane. The origin of the fast transients prior to this electrogenic phase is not clear, but their presence in a fully reduced sample (not shown) implies that they are not related to backflow, but rather to CO photolysis. Apparently, the release of CO from the active site induces some small transient rearrangement in the enzyme's structure. Thus, electron transfer between heme b_3 and heme *b* appears to be nonelectrogenic, which implies that these redox centers reside at similar depths inside the membrane.

The relaxation of the potential is due to the re-formation of the mixed-valence enzyme, caused by the trapping of the electron on heme b_3 by CO binding. The biphasicity of the relaxation is probably due to the existence of mixed-valence enzymes containing two or three electrons. In presence of three electrons, the probability of having an electron on heme b_3 is higher than in the case when only two electrons are present. In the former case, the heme b_3−CO adduct will re-form quicker, so that this population will relax with a higher rate constant.

Electrogenicity: Investigation of Proton Movements

Respiratory Control Ratio. "Respiratory control" implies that the catalysis of a respiratory enzyme is coupled to the generation of a potential across the membrane. Disruption of such a potential by the addition of ionophores and protonophores will cause an increase in the steady-state turnover rate. The relative effect of the uncouplers on activity is represented by the respiratory control ratio (RCR).

For our experiment, NOR was co-reconstituted with the aa_3-type cytochrome oxidase from *P. denitrificans*. Since the cytochrome aa_3 cannot reduce NO under anaerobic conditions at any significant rate (*32*), and oxygen reduction by NOR is very inefficient (*33*), the RCR on the two enzymes can be determined in the same sample. Cytochrome oxidase activity showed a RCR of 3.4 ± 0.2 ($n = 3$).[3] This suggests that the proteoliposomes were sealed well and reconstitution had been effective. In contrast, no respiratory control was found on the NO reducing activity of the same batch of proteoliposomes (RCR of 1.05 ± 0.07, $n = 4$). The total absence of respiratory control suggests that NOR is neither a proton pump nor electrogenic.

Electrometric Steady-State Turnover. We also measured the generation of a membrane potential during steady-state turnover by NOR directly by electrometry on liposomes containing only NOR. No membrane potential was generated during the NO turnover by NOR. After the steady-state experiment, an NO-flow flash experiment was performed (see below) on the same sample, which resulted in the detection of a transient pre-steady-state potential. This implies that the absence of a steady-state potential was not caused by the absence of active enzyme in the sample, or by a problem with the detection (e.g., due to a very fast relaxation of the membrane). Therefore, we conclude that turnover by NOR is electroneutral. This implies that no proton pumping occurs, and that the protons required for catalysis are taken from

[3] Average ± standard deviation.

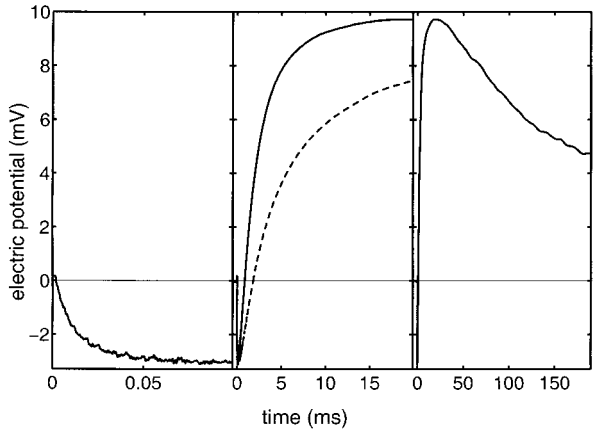

FIGURE 5: Membrane potential development during the reaction of fully reduced NOR with NO on different time scales. The reaction was initiated by a laser flash at 450 ms after the beginning of the injection of 100 μL of NO-saturated buffer. The experimental conditions were the same as listed in Figure 6, except that 20 μM hexaammineruthenium was present.

Table 1: Components of the Transient Potential of the Electrogenic Flow−Flash Response[a]

phase	rate constant (s^{-1})	amplitude (mV)
Lag	5×10^5	−
1: Negative 1	$(2.2 \pm 0.5) \times 10^5$	-1.6 ± 0.5
2: Negative 2	$(4 \pm 0.9) \times 10^4$	-1.0 ± 0.3
3: Negative 3	$(5 \pm 1) \times 10^3$	-0.4 ± 0.5
4: Positive 1	$(6 \pm 1) \times 10^2$	10 ± 3
5: Positive 2	$(1.1 \pm 0.6) \times 10^2$	3 ± 1
6: Decay	6 ± 1	-10 ± 2

[a] Given are the averages and standard deviations of the rate constants and amplitudes (if applicable) of the phases determined by analysis with the sequential reaction model of the responses of four samples.

the same side of the membrane as the electrons, e.g., from the periplasm.

Processes Involved in NO Turnover

We have investigated the turnover of fully reduced NOR in a time-resolved manner by 'flow−flash' experiments to determine when the proton and electron movements occur during turnover, and which intermediates are formed. In such experiments, substrate was added to the fully reduced, CO-inhibited enzyme in the 'flow' phase. Thereafter, the reaction is started by photolysis of the CO with a laser, the 'flash'. In this way, turnover is initiated in-phase in the entire enzyme population.

Electrometric NO Flow−Flash Experiments. A typical electrometric response in the reaction of fully reduced NOR with NO is shown in Figure 5. After a short lag, a transient potential with negative sign develops, followed by the generation of a positive potential, which subsequently decays. The experimental traces were analyzed using a sequential reaction model (see Materials and Methods). This analysis resolves six exponential processes after the initial lag. The rate constants and amplitudes of these phases are listed in Table 1, together with the rate constant of the initial lag. The observation of a phase with a rate constant of only 6 s^{-1} indicates that the membrane relaxation was 6 s^{-1} or less, which implies that the membrane system was sealed well.

The phases are caused by the movement of charges across the membrane dielectric. The topology of the redox centers

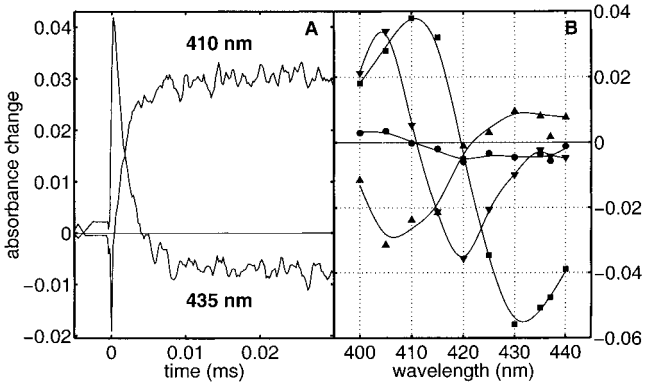

FIGURE 6: Reaction of the fully reduced NOR with NO at room temperature recorded in the Soret region. Panel A shows the initial absorption changes at 410 and 435 nm of the response, that was followed over 5 ms. Zero absorbance corresponds to the CO-inhibited enzyme. The reaction was started by laser flash 100 ms after mixing the sample with saturated NO. After mixing, the sample contained 1.9 μM NOR, in 30 mM K-Hepes, pH 8, 30 mM NaCl, 0.02% DM, 3 mM ascorbate, some dithionite, and 5 μM CO. The right panel shows the kinetic spectra of the four identified phases with the following rate constants: 5×10^5 s^{-1} (■), 1.9×10^4 s^{-1} (●), 1.3×10^3 s^{-1} (▲), and 3×10^2 s^{-1} (▼).

causes electron transport to generate a negative potential or no potential at all. Therefore, the generation of the positive potential is likely to involve proton movements from outside toward the catalytic site. We repeated the electrometric flow−flash experiment in D_2O-containing buffer to identify the phases whose rates are limited by the movement of protons that are in equilibrium with the bulk medium. A clear retarding effect (see Figure 5) of D_2O was observed only on the two positive phases, indicating that these involve the movements of protons toward the inside of the liposomes.

Optical Flow−Flash Experiments. We have performed optical flow−flash experiments on soluble enzyme in a detergent solution to further characterize the turnover process. Fully reduced NOR contains electrons for two turnover reactions. The first turnover is likely to involve only the electrons on the metals in the binuclear site. For the second turnover, the electrons from the low-spin hemes need to move into the active site. Low-spin hemes have easily discernible and intense optical spectra in the alpha band region, whereas changes in the binuclear center are more likely to have spectral signals only in the Soret region. Therefore, we performed the optical flow−flash experiments on a fast time scale (up to 5 ms; see Materials and Methods) in the Soret region, and followed the slower processes in the alpha region.

Four processes that followed the photolysis were resolved in the Soret experiment (Figure 6). The reconstructed spectrum of the first phase (Figure 6B, squares, $k = 4.5 \times 10^5$ s^{-1}) shows a trough at 430 nm and a peak at 410 nm. This spectrum is attributed to the binding of NO to the reduced high-spin heme b_3. The spectrum of the second phase (circles, $k = 1.9 \times 10^4$ s^{-1}) has a very weak spectrum with hardly any amplitude. Since non-heme irons normally have weak spectra, this phase may correspond to a process on Fe_B. The broad trough around 405 nm and plateau around 430 nm in the third phase (triangles up, $k = 1.3 \times 10^3$ s^{-1}) cannot be assigned easily. In contrast, the sharp peak at 405 nm and the trough at 420 nm, observed in the fourth phase (triangles down, $k = 300$ s^{-1}) form a typical heme *c* oxidation spectrum.

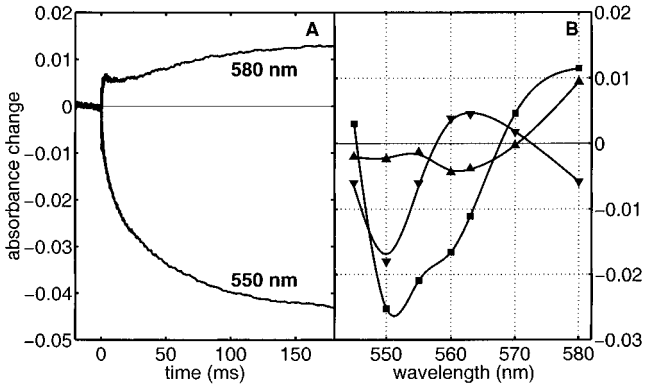

FIGURE 7: Reaction of the fully reduced NOR with NO at room temperature in the alpha band region. Panel A shows the absorption changes at 550 and 580 nm. Zero absorbance corresponds to the CO-inhibited enzyme. The reaction was started by a laser flash 100 ms after mixing the sample with saturated NO. After mixing, the sample contained 6 μM NOR, 60 mM K-Hepes, pH 8, 0.01% DM, 2.5 mM ascorbate, and 50 μM CO. Panel B shows the kinetic spectra of the three identified phases with the following rate constants: 850 s^{-1} (▲), 130 s^{-1} (▼), 14 s^{-1} (■).

Table 2: Phases of the Optical Flow−Flash Responses[a]

phase	rate constant (s^{-1})	spectrum
Optical 1	5×10^5	■ (6B)
Optical 2	1.9×10^4	● (6B)
Optical 3	$(0.85-1.3) \times 10^3$	▲ (6B), (7B)
Optical 4	1.0×10^2	▼ (6B), (7B)
Optical 5	14	■ (7B)

[a] Listed are the rate constant and a reference to the spectrum of each phase.

Performing the experiment over a 200 ms time scale in the alpha band region resulted in the detection of three phases (Figure 7A), with rate constants of 8.5×10^2, 1.0×10^2, and 14 s^{-1}, respectively. The spectrum of the first phase (Figure 7B, triangles up) shows loss of absorbance below 570 nm, and an absorbance increase at higher wavelengths. The sharp trough near 550 nm in the spectrum of the second phase (triangles down) indicates heme *c* oxidation. The spectrum of the third phase (squares) is a combination of oxidation of heme *c* and heme *b*, indicated by the shoulder at 560 nm on the 550 nm trough.

In both experiments, a phase was observed with a rate constant around 10^3 s^{-1}, which was followed by a phase showing oxidation of heme *c*. The whole optical response, combining the two time frames, thus consists of five phases. The rate constant of the heme *c* oxidation as determined in the Soret experiment was 3×10^2 s^{-1}, slightly faster than the 1.3×10^2 s^{-1} determined in the alpha band experiment. The fast time scale in the Soret experiment does not allow the accurate determination of such a comparably slow rate constant. Therefore, the rate constant obtained from the alpha band experiment represents a better estimation of the rate constant for this phase. An overview of the optical phases and their rates is given in Table 2.

DISCUSSION

Our results suggest that the topologies of the redox centers and the electron-transfer pathway are similar in NOR and the oxygen-reducing heme−copper oxidases (Figure 8) (*34*, *35*). The rate constants of electron transfer between the

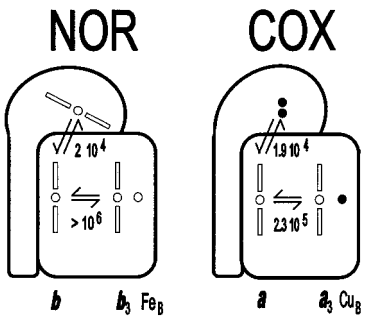

FIGURE 8: Schematic drawings of NOR and CCO. Two bars with an open circle in the middle represent heme. Open circles represent iron atoms, filled ones copper atoms. The names of the metal centers and the rate constants of electron transfer between them are indicated [this work, (*29*)].

electron entry sites and the low-spin heme center (heme *c* and heme *b*, or Cu_A and heme *a*, respectively) are identical. Since the protein packing density, the reorganization energy, and the midpoint potential differences are all likely to be similar, the same rate suggests that the distance between the redox centers is comparable, that is, about 20 Å (*34*, *35*). The distance between the low-spin heme center (cytochrome *b*/cytochrome *a*) and the high-spin heme in the active site is also expected to be similar. The higher rate constant observed for NOR is probably due to the larger difference in midpoint potential of the two centers. The low midpoint potential of heme b_3 also causes the much larger amplitude of the backflow in NOR as compared to that in CCO (*29*).

The midpoint potentials for the redox centers in NOR have been determined by equilibrium redox titrations (*15*). The return of electrons to the binuclear site from low-spin hemes after flash-photolysis is due to the re-formation of the CO-bound enzyme. The relaxation rate equals k·[CO]·[red b_3], in which k is the bimolecular rate constant of CO binding to reduced heme b_3. Since the CO concentration was kept constant, the difference in the relaxation rates is due to the partial oxidation of reduced heme b_3 in the mixed-valence enzyme caused by electron redistribution [see (*20*)]. The reduction level of heme b_3 depends on the difference in the redox potentials of the hemes. Therefore, this potential difference can be determined from the ratio of the relaxation rates of the fully reduced versus the mixed-valence enzyme.

The observed rate constant for CO recombination to reduced NOR (320 s^{-1}) is likely to be an underestimate caused by the low experimental time resolution. A recombination rate of 1700 s^{-1} is expected at 10 μM CO based on the bimolecular rate constant of 1.7×10^8 M^{-1} s^{-1} for the recombination of CO to the reduced NOR (*18*). At this concentration of CO, we observed a recombination rate of 24 s^{-1} for the CO-bound mixed-valence enzyme. Thus, the equilibrium constant of the electron transfer between hemes *c* and b_3 would be about 70, which corresponds to a midpoint potential difference between heme *c* and heme b_3 of about 110 mV. This is less than half of the value determined by equilibrium redox titration [250 mV, (*15*)].

In CCO, the redox centers are negatively cooperative. Reduction of the redox center with the lowest midpoint potential is more difficult when all other redox centers have already been reduced, resulting in a decrease of the apparent midpoint potential by 120 mV [see (*36*)]. The reason for this is the repulsion of the incoming electron by the electrons

that are already present in the other redox centers inside the membrane. The much smaller difference between the midpoint potentials of hemes *c* and b_3, as determined by backflow in partially reduced enzyme, versus the value from the equilibrium titrations indicates that negative cooperativity also exists in NOR.

In liposomes, the turnover of NOR is not coupled to respiratory control. The reaction seems to be uncoupled despite the high driving force of the NO/N_2O couple ($\Delta E_m = +1.12$ V). The generation of a membrane potential was not detected in the electrometric steady-state turnover experiment. In addition, the flow−flash experiment revealed a phase that has a large positive potential and is sensitive to D_2O, suggesting that the substrate protons are taken up from the periplasm. Therefore, we can conclude that the turnover of NOR is electroneutral, in agreement with the results obtained with whole bacterial cells (*16*). The reason for the uncoupled reaction might be that a high turnover rate is essential due to the high toxicity of NO. Coupling of proton pumping and membrane potential generation to the NO-reductive chemistry would slow the turnover. The active site of NOR is predicted to be closer to the periplasm than to the cytosol. Since reduction of the active site is coupled to proton uptake (see below), a short proton uptake pathway down the existing gradient is likely to facilitate the reduction of the active site and thus stimulate turnover numbers.

Catalytic Cycle. The time-resolved measurements of the electric potential and the absorbance changes detect at least five phases during the catalytic cycle, indicating that the turnover is a complex process. We make an attempt to assign all the phases, but remind the reader that this cannot be done with total confidence at the moment. However, two firm conclusions can be drawn from the data. First, the D_2O sensitivity of the positive phases clearly establishes that these involve the uptake of protons from the outside of the liposomes corresponding to the periplasmic side of the bacterial cell membrane. Second, the data further imply that at least one proton is taken up upon reduction of the active site.

NO Binding. CO can bind to heme b_3, but probably not to Fe_B [see, e.g., (*37*, *38*)]. The start of the flow−flash experiment thus involves the removal of the CO molecule from heme b_3. The first phase of the reaction with NO after CO photolysis shows a strong absorbance change characteristic for ligand binding to the reduced high-spin heme. The spectrum of this phase is very similar to the one of NO binding by myoglobin [A. Jasaitis and M. Verkhovsky, data not shown, (*39*)]. So we can conclude that in 2 μs after photolysis a molecule of NO binds to heme b_3. This first phase of NO binding is detected as a lag in the electrometric data (Table 1), which is not surprising because NO is an uncharged molecule, and its binding to heme b_3 is expected to be an electrogenically neutral process.

If the NO molecule that binds is derived from the bulk, this process would depend on the total NO concentration. In this case, the bimolecular binding rate constant for NO to reduced heme b_3 can be estimated to be on the order of 10^9 M^{-1} s^{-1} (5×10^5 s^{-1}/6.5×10^{-4} M). The similar rate constant of the lag in the electrometric response might be due to similar local NO concentrations. However, the hydrophobic character of NO makes it very likely that during the delay between flow and flash (450 ms) substantial partitioning into the lipid phase will occur, giving rise to a much higher local NO concentration around the enzyme in the electrometric experiment. The enrichment should be of the same order of magnitude as the partitioning constant for NO between organic phases and water, which is around 9 (*40*). The similarity between the rate constants of the optical and electrometric NO binding phases ("Optical 1" and the "Lag" in Tables 1 and 2) suggests that the NO binding process is not dependent on the NO concentration in the bulk phase. This could imply that additional NO binding sites exist inside the enzyme. Since Fe_B probably does not bind CO, it is a candidate for such a site.

Intermediates. In the electrometric data, the lag is followed by a negative potential change that can be resolved into three phases (Table 1). The first negative phase (2.2×10^5 s^{-1}) is not detected by optical spectroscopy. This suggests that, for instance, the charge movement could involve small side chain movements inside the active side upon NO binding. In the *trans*-model of de Vries and co-workers (*41*), NO binding to heme b_3 induces the detachment of the proximal histidine. Such a detachment is expected to induce a large optical change in the Soret region, as occurs in the soluble guanylate cyclase (*42*). The lack of a detectable absorbance change during the first negative phase after NO binding to heme b_3 indicates that the heme itself is not perturbed during the initial binding.

The generation of a positive potential of 10 mV ("Positive 1" in Table 1) is attributed to the movement of a single positive charge from the outside of the liposomes into the active site (see below). Assuming that the active site in NOR is at 1/3 of the membrane dielectric of about 40 Å from the periplasmic side, movement of a single charge across 1 Å of the dielectric would thus have generated a potential of ~1.3 mV. The amplitude of the first negative phase would thus require the net movement of a single charge across 2 Å of the dielectric, and an even smaller net movement can account for the second negative phase (Table 1).

The second negative phase has a rate constant similar to the second optical phase (4×10^4 and 1.9×10^4 s^{-1}, respectively). The low intensity of the optical change suggests that this phase might be related to charge movement affecting the ligand on heme b_3, or involving Fe_B. One possibility is that an electron moves from Fe_B to the NO intermediate that is bound to heme b_3.

The amplitude of the third negative phase (5×10^3 s^{-1}) is very small. As no matching optical phase with a similar rate constant has been detected, we attribute this phase to the "silent" formation of a transition state/intermediate, which does not involve charge movements across the membrane dielectric and does not influence the spectrum of the metals in the active site. The silent phase is followed by a new optically detectable change (1×10^3 s^{-1}; "Optical 3" in Table 2). Its spectrum appears to be the combination of the absorbance loss attributed to NO binding (inverse of "Optical 1") and the oxidation of heme b_3 that causes the absorbance change around 435 nm. The α-band spectrum of this phase can be ascribed to the formation of the μ-oxo bridge (*43*) that occurred during this phase. The similarity between the rate constants of the third optical phase and the first positive electrometric phase, that is sensitive to D_2O, may indicate that this process involves the uptake of at least one proton from the outside of the liposomes. The insensitivity of the

resonance Raman frequency to D_2O suggests that the oxo-bridge is not protonated (*43*). Thus, the destination of the uptaken proton is unclear. However, since the uptake is linked to the turnover, the proton is expected to reside close to the active site. Glutamate-198 of NorB, which is thought to reside just below Fe_B inside the protein (*44*), might function as this storage side: recent mutagenesis data have indicated that it is essential for NOR activity (*45*).

The next optically detectable phases show the oxidation of the low-spin hemes. The fourth optical phase, or the 'heme *c* oxidation' phase, is expected to include ca. 20% oxidation of heme *b*, since the midpoint potential of heme *b* is only 35 mV higher than that of heme *c* (*15*). It is not clear why a single electron oxidation is detected in part of the enzyme ("Optical 4", Table 2), whereas another part shows both low-spin hemes oxidized in parallel ("Optical 5"). Neither is the reason known why only about 60% of the low-spin heme *c* oxidized during the measured response (based on the amplitude at 550 nm).

The similarity of the rate constants suggests that the optical phases 4 (130 s^{-1}) and 5 (14 s^{-1}) may correlate to the second positive phase (110 s^{-1}) and the final decay (6 s^{-1}), respectively. The spectrum of the fourth optical phase reveals that heme *c* is oxidized (this phase probably included partial heme *b* oxidation as well, see above). As the second positive phase is sensitive to D_2O, it involves proton movement. Therefore, the generation of a positive potential during this phase can be explained, if the completion of catalysis during the first positive phase has only involved the uptake of a single proton, so that another proton can be taken up upon one-electron reduction of the active site. Proton uptake as a charge compensation upon reduction of the active site occurs in cytochrome oxidases (*46*). In NOR, the uptake of one (or two) proton(s) in parallel to the reduction of the active site could also be needed for the release of the μ-oxo-bridge as a hydroxide ion (or water molecule). The bridge is not present in the reduced active site (*41*). The fifth optical phase is coupled to the oxidation of heme *b* and heme *c*. Oxidation of both low-spin hemes in parallel to the uptake of a single proton would be electroneutral.

The total reaction results in an overall positive potential. This is not in disagreement with the electroneutrality of NOR's turnover, since the reaction has been started with the fully reduced enzyme. The reduction of the active site is coupled to proton uptake. The complete reduction will involve transfer of three electrons and one or two protons into the membrane from the same direction, which will generate a net negative potential. The electroneutrality thus implies that oxidation of the enzyme should result in the generation of a potential of opposite sign and identical amplitude.

Rereduction of the active site in NOR is likely to involve the arrival of electrons and protons, which are trapped there by NO, so that this process is sensitive to D_2O as well as to the local concentration of NO. Since the latter is expected to be higher in the electrometric experiments than in the optical experiments, the rate constants of these processes may well be higher in the first set of data. Based on this, a model can be presented for the rereduction phases, in which the last two optical phases correlate to the two subsequent positive phases (the electrometric rate constants are a factor of 5 faster than the optical ones; see Tables 1 and 2). In this model, the completion of the first catalytic cycle during the third positive phase is seen as an electroneutral process that does not have any proton uptake associated with it. Instead, the uptake of both protons is thought to occur upon reduction of the active site—one proton taken up with each electron. Thus, reduction of the active site with an electron coming from heme *c* would always be electroneutral, whereas oxidation of heme *b* always gives rise to a positive potential. The positive potentials attributed to the optical phases 4 and 5 would always be related to oxidation of heme *b*. The decay phase is attributed entirely to membrane relaxation.

Mechanism of NO Reduction. Two types of mechanisms have been discussed for reduction of NO. The mechanism involves either the binding of one molecule of NO to each metal center in the binuclear site ('trans' mechanism) or the binding of both NO molecules to only one of the metals ['cis' mechanism; see (*47*)]. In the trans mechanism (*5, 41*), the reaction starts with a fully reduced binuclear site, onto which one molecule of NO binds to each of the metals in the active site. A detailed model of a cis mechanism has been suggested for the reduction of NO by the cytochrome bo_3 quinol oxidase from *E. coli* (*48*). Here the reaction starts with the binding of two NO molecules to the Cu_B in the oxidized binuclear center. NO binding to the heme iron is not part of the catalytic cycle. A similar mechanism involving Fe_B has been suggested for NOR (*49*).

Our data are not sufficient to discriminate between the two mechanisms, even though the assigment of NO binding to the reduced heme b_3 in the first 2 μs of the reaction is in contradiction with the cis model, and would be in agreement with the trans model. Our results open up the possibility of a cis mechanism involving heme b_3: the silent negative phase ("Negative 3" in Table 1, 5000 s^{-1}) could represent a step between the charge movements in the active site and the completion of the first catalytic cycle during the third optical phase ("Optical 3" in Table 2, 850−1300 s^{-1}), as suggested above. However, since the rate constant of "Negative 3" is about a factor of 5 faster than that of "Optical 3", both phases might also be caused by the same, NO-dependent process. This would imply that the second molecule of NO only binds to the active site at completion of the first catalytic cycle. Such a mechanism in which the two molecules of NO interact with the active site heme during the catalytic cycle is thought to occur in the fungal NO reductase, called P450nor (*50, 51*). These enzymes are soluble P450-type enzymes that contain only one cysteine-liganded *b*-type heme in their active site (*10*).

REFERENCES

1. van der Oost, J., deBoer, A. P. N., deGier, J.-W. L., Zumft, W. G., Stouthamer, A. H., and van Spanning, R. J. M. (1994) *FEMS Microbiol. Lett. 121*, 109.
2. Saraste, M., and Castresana, J. (1994) *FEBS Lett. 341*, 1−4.
3. de Boer, A. P., van der Oost, J., Reijnders, W. N., Westerhoff, H. V., Stouthamer, A. H., and van Spanning, R. J. (1996) *Eur. J. Biochem. 242*, 592−600.
4. Heiss, B., Frunzke, K., and Zumft, W. G. (1989) *J. Bacteriol. 171*, 3288−3297.
5. Girsch, P., and de Vries, S. (1997) *Biochim. Biophys. Acta 1318*, 202−216.
6. Cheesman, M. R., Zumft, W. G., and Thomson, A. J. (1998) *Biochemistry 37*, 3994−4000.
7. Hendriks, J., Gohlke, U., and Saraste, M. (1998) *J. Bioenerg. Biomembr. 30*, 15−24.

8. Cramm, R., Siddiqui, R. A., and Friedrich, B. (1997) *J. Bacteriol. 179*, 6769−6777.
9. Cramm, R., Pohlmann, A., and Friedrich, B. (1999) *FEBS Lett. 460*, 6−10.
10. Hendriks, J., Oubrie, A., Castresana, J., Urbani, A., Gemeinhardt, S., and Saraste, M. (2000) *Biochim. Biophys. Acta 1459*, 266−273.
11. Zafiriou, O. C., Hanley, Q. S., and Snyder, G. (1989) *J. Biol. Chem. 264*, 5694−5699.
12. Goretski, J., Zafiriou, O. C., and Hollocher, T. C. (1990) *J. Biol. Chem. 265*, 11535−11538.
13. Koutny, M., and Kucera, I. (1999) *Biochem. Biophys. Res. Commun. 262*, 562−564.
14. Sakurai, N., and Sakurai, T. (1998) *Biochem. Biophys. Res. Commun. 243*, 400−406.
15. Gronberg, K. L., Roldan, M. D., Prior, L., Butland, G., Cheesman, M. R., Richardson, D. J., Spiro, S., Thomson, A. J., and Watmough, N. J. (1999) *Biochemistry 38*, 13780−13786.
16. Bell, L. C., Richardson, D. J., and Ferguson, S. J. (1992) *J. Gen. Microbiol. 138 (Pt. 3)*, 437−443.
17. Warne, A., Wang, D. N., and Saraste, M. (1995) *Eur. J. Biochem. 234*, 443−451.
18. Hendriks, J. H. M., Saraste, M., and Watmough, N. J. (2001) *Biochemistry* (in press).
19. Morgan, J. E., Verkhovsky, M. I., Puustinen, A., and Wikström, M. (1995) *Biochemistry 34*, 15633−15637.
20. Morgan, J. E., Verkhovsky, M. I., Puustinen, A., and Wikström, M. (1993) *Biochemistry 32*, 11413−11418.
21. Rigaud, J.-L., Pitard, B., and Levy, D. (1995) *Biochim. Biophys. Acta 1231*, 223−246.
22. Kocur, M. (1984) in *Bergey's manual of systematic biology* (Krieg, N. E. D., Ed.) pp 399−402, Williams & Wilkins, Baltimore, MD.
23. Rigaud, J. L., Mosser, G., Lacapere, J. J., Olofsson, A., Levy, D., and Ranck, J. L. (1997) *J. Struct. Biol. 118*, 226−235.
24. Drachev, L. A., Jasaitis, A. A., Kaulen, A. D., Kondrashin, A. A., Liberman, E. A., Nemecek, I. B., Ostroumov, S. A., Semenov, A. Y., and Skulachev, V. P. (1974) *Nature 249*, 321−324.
25. Drachev, L. A., Kaulen, A. D., Semenov, A. Y., Severina, I. I., and Skulachev, V. P. (1979) *Anal. Biochem. 96*, 250−262.
26. Verkhovsky, M. I., Morgan, J. E., Verkhovskaya, M., and Wikstrom, M. (1997) *Biochim. Biophys. Acta 1318*, 6−10.
27. Jasaitis, A., Verkhovsky, M. I., Morgan, J. E., Verkhovskaya, M. L., and Wikstrom, M. (1999) *Biochemistry 38*, 2697−2706.
28. Oliveberg, M., and Malmström, B. G. (1991) *Biochemistry 30*, 7053−7057.
29. Verkhovsky, M. I., Morgan, J. E., and Wikström, M. (1992) *Biochemistry 31*, 11860−11863.
30. Einarsdóttir, O., Georgiadis, K. E., and Sucheta, A. (1995) *Biochemistry 34*, 496−508.
31. Boelens, R., Wever, R., and Van Gelder, B. F. (1982) *Biochim. Biophys. Acta 682*, 264−272.
32. Stubauer, G., Giuffre, A., Brunori, M., and Sarti, P. (1998) *Biochem. Biophys. Res. Commun. 245*, 459−465.
33. Fujiwara, T., and Fukumori, Y. (1996) *J. Bacteriol. 178*, 1866−1871.
34. Tsukihara, T., Aoyama, H., Yamashita, E., Tomizaki, T., Yamaguchi, H., Shinzawa-Itoh, K., Nakashima, T., Yaono, R., and Yoshikawa, S. (1995) *Science 269*, 1069−1074.
35. Iwata, S., Ostermeier, C., Ludwig, B., and Michel, H. (1995) *Nature 376*, 660−669.
36. Wikstrom, K. F., Harmon, H. J., Ingledew, W. J., and Chance, B. (1976) *FEBS Lett. 65*, 259−277.
37. Flatman, S., Hurst, J. S., McDonald-Gibson, R. G., Jonas, G. E., and Slater, T. F. (1986) *Biochim. Biophys. Acta 883*, 7−14.
38. Hendriks, J., Warne, A., Gohlke, U., Haltia, T., Ludovici, C., Lubben, M., and Saraste, M. (1998) *Biochemistry 37*, 13102−13109.
39. Seward, H. E. T. (1999) *Magnetooptical spectroscopy of hemoproteins*, Ph.D. Thesis, University of East Anglia.
40. Shaw, A. W., and Vosper, A. J. (1977) *J. Chem. Soc., Faraday Trans. 1 8*, 1239−1244.
41. Moënne-Loccoz, P., and de Vries, S. (1998) *J. Am. Chem. Soc. 120*, 5147−5152.
42. Zhao, Y., Brandish, P. E., Ballou, D. P., and Marletta, M. A. (1999) *Proc. Natl. Acad. Sci. U.S.A. 96*, 14753−14758.
43. Moënne-Loccoz, P., Richter, O.-M. H., Huang, H., Wasser, I. M., Ghiladi, R. A., Karlin, K. D., and de Vries, S. (2000) *J. Am. Chem. Soc. 122*, 7618−7619.
44. Kannt, A., Michel, H., Cheesman, M. R., Thomson, A. J., Dreusch, A. B., Körner, H., and Zumft, W. G. (1998) in *Biological electron-transfer chains: genetics, composition and mode of operation* (Canters, G. W., and Vjigenboom, E., Eds.) pp 279−291, Kluwer Academic Press, Dordrecht/Boston/London.
45. Butland, G., Spiro, S., Watmough, N. J., and Richardson, D. J. (2001) *J. Bacteriol. 183*, 189−199.
46. Mitchell, R., and Rich, P. R. (1994) *Biochim. Biophys. Acta 1186*, 19−26.
47. Ye, R. W., Averill, B. A., and Tiedje, J. M. (1994) *Appl. Environ. Microbiol. 60*, 1053−1058.
48. Butler, C. S., Seward, H. E., Greenwood, C., and Thomson, A. J. (1997) *Biochemistry 36*, 16259−16266.
49. Watmough, N. J., Cheesman, M. R., Butler, C. S., Little, R. H., Greenwood, C., and Thomson, A. J. (1998) *J. Bioenerg. Biomembr. 30*, 55−62.
50. Shiro, Y., Fujii, M., Isogai, Y., Adachi, S., Iizuka, T., Obayashi, E., Makino, R., Nakahara, K., and Shoun, H. (1995) *Biochemistry 34*, 9052−9058.
51. Obayashi, E., Takahashi, S., and Shiro, Y. (1998) *J. Am. Chem. Soc. 120*, 12964−12965.

BI0121050